JOURNAL OF PROPULSION AND POWER
Vol. 9, No. 3, May–June 1993

High-Temperature Supersonic Combustion Testing with Optical Diagnostics

T. E. Parker,* M. G. Allen,* W. G. Reinecke,* H. H. Legner,* R. R. Foutter,† and W. T. Rawlins‡
Physical Sciences, Inc., Andover, Massachusetts 01810

The development of supersonic combustion ramjet (SCRAMJET) engines requires testing using new, nonintrusive, instrumentation methods in high-speed, high-enthalpy flow facilities. The stagnation temperatures for very high flight speeds (in excess of 3000 K) make the production of these flows impossible using conventional methods such as resistance heaters or vitiated flows. Similarly, measurements of properties in these flows is difficult since the measurement must be nonintrusive in nature. This article describes a test series using a shock tunnel to produce Mach 3.0 flows with stagnation temperatures in excess of 3000 K and an optical diagnostic set specifically tailored for measurements in supersonic high temperature systems. The test facility includes a hydrogen injection capability which makes combustion tests possible for these flows. This article describes the shock tunnel and its capabilities, provides an overview of the optical diagnostics used in the testing, and discusses the results of both combusting and noncombusting tests.

Introduction

THE development of hypersonic vehicles based on supersonic combustion ramjet (SCRAMJET) propulsion requires testing in high-enthalpy flow facilities using nonintrusive diagnostic measurements. Shock tunnels are one method of producing these high-enthalpy flows, and optical diagnostic techniques offer a unique opportunity to probe the high temperature and velocity flow. The application of these rapidly maturing nonintrusive measurements to high-enthalpy combusting flows is a subject of direct relevance to the development of thrust systems for high-speed flight. Recent work[1–5] has addressed several of the diagnostic issues associated with high-speed reacting flows. This article details results from an initial test series using a shock tunnel to produce Mach 3.0 flows with stagnation temperatures in excess of 3000 K and an optical diagnostic set specifically tailored for measurements in supersonic high-temperature systems. A hydrogen injection capability was included which makes combustion tests possible. The optical measurements include both spatially resolved and line-of-sight-averaged concentration and temperature measurements. This article describes the development and performance of a shock-tunnel facility capable of simulating high-speed flight conditions, provides a discussion of the optical diagnostic techniques which were developed for this facility, and presents a series of test results for both noncombusting and combusting flows.

Experimental Facility Description

The experimental facility includes a shock tunnel configured to produce Mach 3.0, high-temperature flows, and a system that injects gas (helium or hydrogen) into these flows. This section describes the shock-tube and tunnel-flow section and the injection system and its performance.

Figure 1 illustrates the major components of the shock-tunnel facility. The shock-tube driver consists of a 160-mm i.d., 203-mm o.d., 3.6-m-long 4140 steel tube fitted with an end cap/fill hose assembly on one end and threaded to accept a connection flange on the other end. The system is designed to routinely withstand pressures of 24 MPa. A vacuum and driver gas supply system are connected to the driver for evacuation and gas-filling purposes. The diaphragm station for the shock tube is a dual diaphragm system which uses 228-mm-square diaphragms that are prepared by mechanically scoring an "x" to enhance petal formation and retention.

The driven section of the shock tube consists of 160-mm i.d. stainless steel tubing with a total length of 13.9 m. This section of the tube is equipped with a high-quality vacuum system capable of 10^{-4}-Pa operation and an accurate gas filling system. The shock tube is used to drive the flow in the shock tunnel and the tunnel is operated in the reflected shock mode. Driver and driven gases for the system are helium and air, respectively; the system is not operated in a tailored interface mode, and the stagnation conditions for the system are controlled by the fill pressure in the driven section and the pressure ratio for the driver to driven section.

The tunnel test section is attached to the end of the shock tube through a series of three flanges that include a secondary diaphragm used to initially separate the shock tube from the tunnel. The transition between the shock tube and tunnel occurs at the shock-tube end wall, which contains a 115-mm-diam opening in the 160-mm i.d. tube. The tunnel flow section is 76.2-mm wide by 89-mm high, and the transition from shock tube to tunnel occurs in a 38-mm-long piece which changes smoothly from a 115-mm i.d. to a rectangular cross section exactly matched to that of the shock tunnel. The secondary diaphragm is held with four dowel pins on the tunnel side of this transition; this diaphragm is typically 0.25-mm brass shim stock scored with an x to enhance petal formation. The purpose of this diaphragm is to isolate the tunnel flow section from the driven section of the shock tube. Vacuum conditions

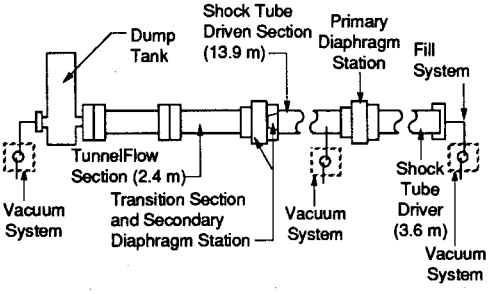

Fig. 1 Schematic diagram of shock-tunnel facility.

Presented as Paper 92-0761 at the AIAA 30th Aerospace Sciences Meeting and Exhibit, Reno, NV, Jan. 6–9, 1992; received Feb. 18, 1992; revision received Sept. 15, 1992; accepted for publication Sept. 25, 1992.

*Principal Research Scientist, 20 New England Business Center. Member AIAA.
†Senior Scientist, 20 New England Business Center. Member AIAA.
‡Principal Research Scientist, 20 New England Business Center.

can therefore be maintained in the tunnel flow section prior to the arrival of the incident shock wave. The tunnel flow starts when the pressure rise in the reflected shock plenum breaks the secondary diaphragm.

The shock-tunnel flow section bolts to the end wall of the shock tube using a series of flanges, and the entire flow section/dump tank assembly is on rollers so that the secondary diaphragm station can be opened and the diaphragm changed. As previously described, the internal cross section of the tunnel flow section is 76.2-mm wide by 89-mm high. An interchangeable, two-dimensional, Mach 3.0 303 stainless steel nozzle block bolts into the interior of the tunnel flow section. The nozzle throat extends across the full width of the shock tunnel, 76.2 mm, is 15.5-mm high and is positioned 19-mm downstream of the secondary diaphragm station. The nozzle is designed to produce uniform velocity Mach 3.0 flow, and 115 mm after the full expansion point terminates in a 12.7-mm-high rearward-facing step.

The shock tunnel itself is made from 304 stainless steel with an approximate wall thickness of 25 mm. It consists of two sections totaling 2.4 m in length, and is held together with 280-mm diam, 38-mm-thick flanges. The tunnel was manufactured to produce as few flow nonidealities as possible. The sections were vacuum brazed together using annealed ground plate. The result is a sharp-cornered internal rectangle with high dimensional accuracy. A sample section of the 304 stainless steel braze joint was destructively tested to verify its strength which was found to be much more than adequate (calculated internal pressure required to produce a failure at the joint was in excess of 40 MPa). The shock tunnel includes both wall-mounted pressure taps and flush-mounted optical window ports. Four of the nine total pressure taps are located in the nozzle expansion region and can be used to verify proper performance of the nozzle. The remainder of the pressure tap locations are located in the region immediately surrounding the injection/combustion region and at subsequent downstream locations. Five axially located optical access stations are included in the shock tunnel and all locations provide access in two orthogonal directions so that line-of-sight and spatially resolved measurements can be made. The first optical port is immediately after the full expansion point for the nozzle and includes three 44.5-mm clear aperture windows. The first three optical access ports are shown schematically in Fig. 2. The region immediately after the rearward-facing step includes two side windows that give full height optical access for a 140-mm flow length. A complementary top window in this region can be used for laser access. The next three optical stations are located 0.29, 1.25, and 1.84 m from the rearward-facing step and consist of 89 mm clear aperture windows on the sides complemented by top and bottom 44 mm clear aperture windows.

Following the shock-tunnel flow section is a dump tank with vacuum system. This tank is a 0.9 m^3 vertical compressed air tank (1.4 MPa working pressure) modified to bolt to the shock tunnel using a 152-mm-diam pipe. The entire dump tank and shock-tunnel assembly ride on rollers to facilitate changing the secondary diaphragm.

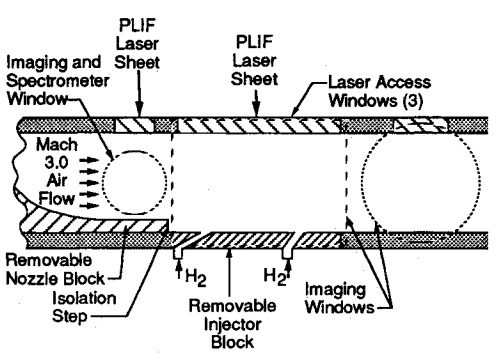

Fig. 2 Optical access in the shock tunnel.

The shock tunnel includes provisions for hydrogen injection so that reacting flows may be studied. As shown in Fig. 2, an interchangeable injector block is included immediately after the rearward-facing step (12.7-mm high) produced by the end of the Mach 3.0 nozzle. The interchangeable injector block can be used to test a variety of injector configurations.

To produce reacting flows similar to those in a scramjet, hydrogen must be injected into the shock-tunnel flow. The requirements for this are pulsed operation with a fast response time, near-constant injection flow rates during the shock-tunnel run time, and a fail-safe method of limiting the quantity of hydrogen injected into the system. We have addressed these requirements using a 3.8 l, 20-MPa-rated bladder accumulator with a custom manufactured, explosive burst diaphragm and manifold system. A dual-diaphragm system separates the nitrogen pressurized hydrogen from the delivery system for the injector block. Injection is possible on demand by simply igniting a hydrogen/oxygen mixture contained between the diaphragms with a spark plug. Testing of this system revealed that initiation times of 800 μs were routinely produced. The injection system can therefore be triggered using one of the pressure transducer signals from the shock tube.

The performance of the injection system is directly relevant to the combustion performance in the shock tunnel. To characterize this system the overall stoichiometry for the system can be calculated in addition to the momentum flux ratios. The overall stoichiometry for the combusting system can be easily described since the injectors in the combustion zone are configured to produce sonic flow at their exit. For a given flow condition and injector area, the stoichiometry is linearly related to the injection pressure. The expected penetration of the injectant plume is also a variable of interest since the injectant must penetrate significantly into, and interact with, the freestream. Injection penetration has been previously studied for crossflows with the injector oriented at 60–120-deg angles with respect to the mainstream flow direction and has been shown to scale with the square root of injectant to freestream stagnation pressure ratio.[6] Although our flow is not a simple jet into a crossflow, we have used the results of Ref. 6 to crudely estimate the midpoint height of the Mach disk to be 6-mm above the tunnel floor. Our schlieren measurements were unable to resolve the location of the Mach disk but we do show enough penetration to produce a bow shock in front of the injectant jet. Injection systems are also categorized by the momentum flux ratio of the injectant to the freestream. For this system, the perpendicular fraction of momentum with respect to the freestream was used to calculate momentum flux, and the momentum flux ratio was 2.0 for the helium injectant and 1.6 for the hydrogen injectant.

For the specific injector configuration used in this work, the injection parameters may all be quantified. The injector ports were located in the tunnel floor after the rearward-facing step along the tunnel centerline at 2.3 and 8.4 step-heights downstream, and are directed at 30- and 60-deg angles with respect to the tunnel flow. Both holes were 4.8 mm in diameter, in all cases injectant pressure was 2 MPa, and the resulting equivalence ratio for the reported test series is 1.6–1.8. The expected penetration height for the Mach disk was 6-mm above the tunnel floor, and the momentum flux ratio for all of the mixing and combustion tests was approximately 2.0 with a helium injectant and 1.6 for a hydrogen injectant.

Shock-Tunnel Performance

The actual performance for the shock tunnel, in terms of test times available—static and stagnation temperatures and pressures that can be achieved, and simulation capability for high speed flight—is described in this section. The range of static temperatures and pressures which can be achieved in the tunnel is illustrated in Fig. 3. The operating zone shown in this figure includes the effects of air chemistry in the reflected shock zone which acts to depress the temperatures which are initially produced. Results for Fig. 3 were calculated

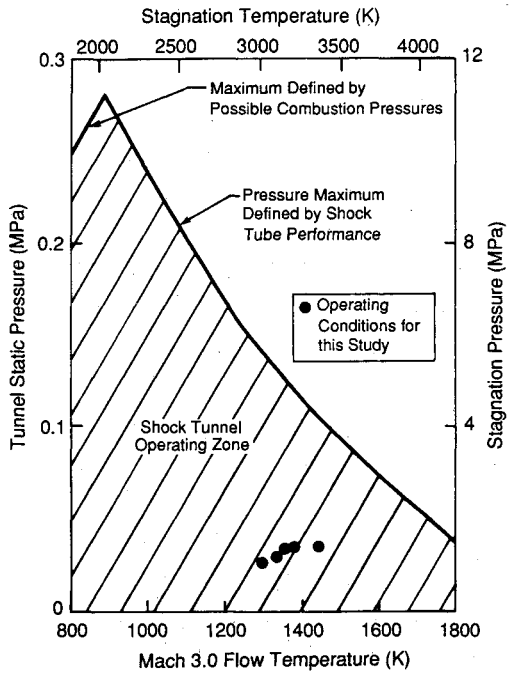

Fig. 3 Shock tunnel operating pressures and temperatures for a helium driver and air as the driven gas.

using incident shock speeds that have routinely been produced in this shock tube to determine the "frozen" or no-reaction temperature; an equilibrium temperature was then calculated by considering the system to be a constant pressure and energy system which reacts to completion. This temperature is the stagnation temperature for the flow and our predicted maximum pressures are set by the maximum pressure in the driver, 18 MPa, the reflected shock-to-driver pressure ratio which is a function of shock speed and a pressure reduction factor which we have empirically observed for this tube. These calculations assume a helium driver and air as the driven gas. Higher flow pressures can be achieved by using hydrogen/helium mixtures as the driver gas. The time required to reach an equilibrium temperature was computed using the CHEMKIN chemical kinetics package[7] and was found to be less than 0.18 m/s for temperatures above 3000 K. Figure 3 also includes conditions that were realized as a part of this study. Pressure and temperature for these conditions were calculated using the incident shock speed. Flow pressures were verified with pressure transducers in the tunnel and the flow temperature was verified using an NO emission diagnostic. Since the relationship between static and stagnation temperatures and pressures for Mach 3.0 flow is a simple multiplicative factor (assuming a specific heat ratio of 1.32), a second set of axes is included which describe the range of stagnation conditions which can be produced. As expected, the maximum pressure drops as the flow temperature increases. This is simply explained by noting that the temperature in the shock tunnel is controlled by the driver-to-driven pressure ratio in the shock tube and that higher temperatures require larger pressure ratios. Since the driver pressure was limited to 17 MPa, the initial pressure in the driven tube, and therefore, the pressure produced by the reflected shock is reduced for higher temperature conditions.

Figure 4 illustrates the flight simulation capabilities for the shock tunnel compared to a proposed flight corridor adopted from Billig.[8] Clearly, the shock tunnel is capable of simulating flight speeds below 3 km/s in the lower pressure regions of the flight corridor. Also included in this figure is the initial testing region for the results described in this work. In terms of the Reynolds number for the flows in the tunnel, a maximum value of 6×10^7/m can be produced for static temperatures of 800 K and 9×10^6/m for static temperatures of 1500

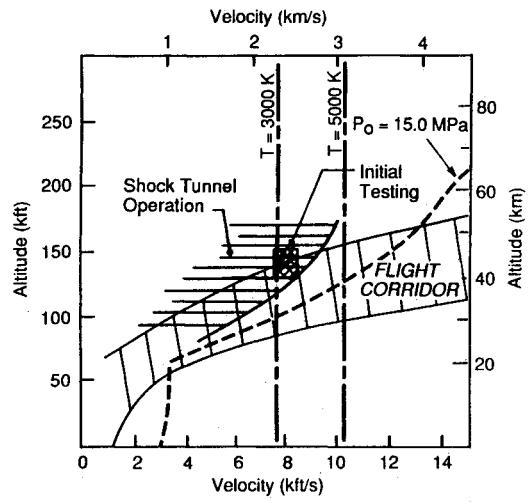

Fig. 4 Shock tunnel operating envelope compared to a flight corridor.

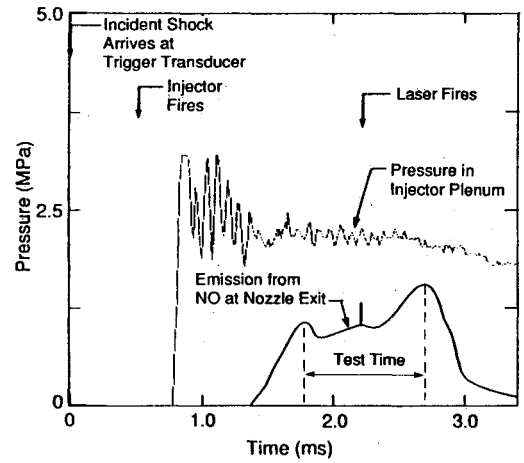

Fig. 5 Timing diagram for shock-tunnel operation.

K. Lower Reynolds numbers may be produced by simply operating the tunnel at lower pressures.

A critical performance parameter for impulse facilities, such as this shock tunnel, is the time duration of the high enthalpy flow which is produced. Test times are determined by monitoring the NO emission near 5.26 μm and were found to be between 1–3 ms for static flow temperatures between 1600–1000 K. The NO emission monitor is ideal for defining the test time in the shock tunnel since the start of NO emission and the start of the flow coincide and the end of the hot flow in the tunnel coincides with a steep drop in the NO emission signal. Figure 5 illustrates a typical test time for the system. The operation of the facility also requires attention to timing and triggering issues; the injection and laser system must be fired at appropriate times to produce injection slightly before the beginning of the flow and a laser pulse during a relatively stable period during the event. This timing sequence is illustrated in Fig. 5 which shows the pressure in the injection system manifold immediately upstream of the injectors and the emission from NO at 5.25 μm. Also included in this figure are the arrival times for the incident shock at the triggering pressure transducer and the triggering times for the injection system and laser.

The previous paragraphs have discussed the operating conditions for the tunnel assuming that the supersonic nozzle performs in a constant manner (i.e., produces Mach 3.0 flow). In addition to schlieren measurements which indicate a Mach 3.0 freestream, the pressure measurements in the nozzle confirm the production of a Mach 3.0 flow.

This section has described the performance for the shock tunnel which was developed as a part of this work. The tunnel

is capable of producing flows very relevant to high speed flight (up to 3 km/s) and in addition is very versatile in term of the range of conditions which can be created. This capability, in conjunction with the injection system for creating mixing/reacting flows and the large optical access, make this facility ideal for studying high enthalpy combustion systems for high-speed flight.

Optical Diagnostic Methods

A major thrust for this work was to demonstrate a series of optical measurements in mixing and/or reacting high-enthalpy flows. These measurements included schlieren imaging, the development of an infrared emission measurement system capable of monitoring temperature and number density of NO, and planar-laser-induced fluorescence (PLIF) measurements of both NO and OH in the injection region. The details of the development and operation of these diagnostics systems are described in detail elsewhere[9,10]; a brief summary of the techniques is included in the following paragraphs.

The diagnostic strategies used in this work, in addition to the standard schlieren measurements, relied on the presence of NO and OH molecules. NO is routinely present in mole fractions greater than 1% for these flows since it is formed in the high temperature plenum region of the shock tube. We performed kinetic studies using a stream-tube simulation of the shock-tunnel nozzle and found that NO does not recombine significantly (NO mole fractions were predicted to decrease in the nozzle by 10–25% for initial temperatures of 2500–4500 K in the plenum). The recombination that is observed occurs only in the high-pressure, low-velocity regions of the nozzle. We can therefore use NO as a tracer molecule for flows without injection, and NO can be considered to be constant in mole fraction in the fully expanded regions of the flow. For flows with hydrogen injection, OH is a particularly appropriate molecule since it is a definitive indicator of combustion. For this work, OH PLIF measurements were used to identify reaction zones between the hydrogen and air.

The infrared emission from the fundamental band of NO near 5.3 μm provides an excellent means of nonintrusively monitoring the flow produced in the shock tunnel. The temperature of the flow in the tunnel, as with other high enthalpy flow facilities, is calculated using one-dimensional gasdynamic relationships which relate conditions in a Mach 3.0 flow to those in the plenum. This calculation assumes idealized processes in the shock-tube plenum and nozzle. Therefore, a real-time monitor of the flow temperature and NO concentration would serve to confirm the calculated flow conditions and continuously assess the character of the Mach 3.0 flow. The motivation for this diagnostic is therefore quite clear, it will accurately quantify the flow conditions in the Mach 3.0 flow.

As described in detail in a companion paper,[10] simultaneous observation of the bandshape and the absolute radiance from vibrationally excited NO provides the column density (integral of number density along the line-of-sight) and path-averaged vibrational temperature of NO in the flowfield. Spectrally resolved emission from the entire band was observed using a specially constructed infrared array spectrometer, consisting of a 12-element HgCdTe linear detector array interfaced to a monochromator. Each pixel in the array has a dedicated amplifier and digitizer which allows synchronous collection of spectra at 125 kHz. Absolute responsivity calibrations were performed with a temperature-controlled blackbody source, and the observed radiances and bandshapes were calibrated for NO number density and vibrational temperature in the reflected shock region of a conventional, 104-mm (i.d.) shock tube.

Results from this calibration allow the calculation of both temperature (based on the relative shape of the spectra) and concentration. Details of this measurement technique are reported elsewhere[10]; results from these measurements on the shock tunnel provide good agreement between the mean temperature which was observed and the predicted temperature based upon plenum conditions and one-dimensional gasdynamics. However, the measured temperatures in the tunnel flow section were observed to fluctuate about this mean value by as much as $\pm 10\%$. This type of fluctuation has been observed in other shock-tunnel flow facilities[11] and its presence underscores the importance of time-resolved, nonintrusive measurements of the flow temperature.

Imaging measurements for this work included both schlieren and PLIF data. Schlieren measurements of flowfields have been widely used for many decades and are a direct indicator of density variations in the flow. Therefore, these images are exceptionally appropriate for defining the position of shocks in the flow. The system used to obtain the images for this work consisted of a xenon flash lamp with arc size and duration of 3 mm and 2 μs, respectively, and a pair of 100-mm diam, 600-mm focal length mirrors. All schlieren images included the full height (89 mm) of the shock tunnel in the injector region.

PLIF images of the flow were also acquired as a part of this work and a full discussion of the technique is included elsewhere.[9] In brief, a laser sheet with a wavelength tuned to exactly coincide with an absorption feature of a molecular constituent in the flow is directed across the tunnel. A gated, intensified camera system is positioned so that an image of the laser sheet may be acquired. Absorption by the molecular component which has been chosen results in fluorescence, and the red-shifted fluorescence is acquired as an image. Careful selection of the absorption transition and a priori knowledge of the nonradiative quenching behavior of the excited state allow the development of specific diagnostic strategies that will produce images of the temperature, number density, or mole fraction in the flow. These strategies are carefully discussed in Ref. 9. For this work, the NO PLIF measurements were primarily sensitive to temperatures, and the OH PLIF measurements were sensitive to number density.

Experimental Results

Both the schlieren and PLIF measurements create images of certain properties in the flowfield and it is instructive to compare these images with predictions of the major features of the flow. Figure 6 illustrates the expected flow over the rearward-facing step. Certain aerodynamic features of the flow are immediately apparent. The interaction of the supersonic flow with the step creates an expansion fan that begins at the step corner with a leading edge oriented with a 19.5-deg angle ($\sin^{-1}$ 1/M) to the flow. The expansion fan extends from this beginning ray to a uniform flow region. On the other edge of the uniform flow region is a recirculation zone whose extent can be estimated from previous results.[12–15] A recompression shock is introduced by the wall and turns the flow once again so that it proceeds directly down the duct.

The flowfield after the rearward-facing step with injection is more complex and a detailed estimate of the features of this flow is beyond the scope of this work. However, general features of this flow may be predicted by simply overlaying

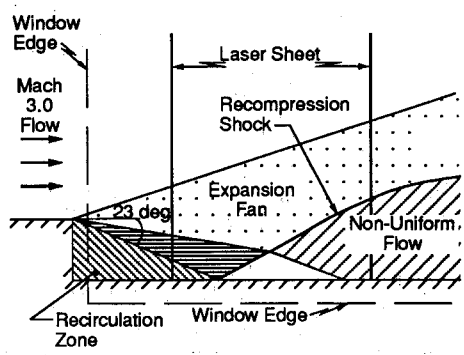

Fig. 6 Graphic representation of the flowfield in the shock tunnel without injection.

an injectant plume on the flow prediction just described. This prediction will be valid only along the centerline of the tunnel which includes the centerline of the injector. For regions not along the tunnel's longitudinal centerline, the flowfield will be some combination of the no-injectant flow and the flow with injection. Figure 7 illustrates this global flow prediction and illustrates the major flow features. The injectant plume will produce a bow shock in a similar fashion to that produced by a solid body in a supersonic flow. Following this shock will be the plume itself and a thin mixing region where the injectant and air meet. The plume, initially oriented at a 30-deg angle to the flow, will spread as it proceeds downstream and will gradually align itself with the flow. The region underneath the plume will consist of a mixture of injectant gas and air from the freestream.

Figures 8 and 9 illustrate the schlieren and NO PLIF images of the flow without injection. Figure 8 is a full-height (89-mm) image of the shock tunnel, the left corner of this image is 30-mm downstream of the rearward-facing step. Features in this image such as the dark horizontal streak, the dark bumps at the bottom of the image, and the circular arc at the left of the image are due to window imperfections only. Figure 9 represents a region of the flow starting 20-mm from the rearward-facing step, extending for 28-mm along the flow length and 29-mm high. Both images clearly show the recompression shock. The comparison shows the fundamental difference between the spatially resolved PLIF image and the schlieren image. As shown in the schlieren photograph, the shock appears to be feathered. This result can be attributed to the path length integration across the flowfield which is inherent in standard schlieren measurements (i.e., the recompression shock is apparently wavy in a direction perpendicular to the flow). The pump transition for the PLIF image was $Q_{22} + R_{12}(7)$. The position of the shock at the exact centerline of the tunnel is determined since the measurement volume is defined by the intersection of the laser sheet and the imaging area. As expected, this view does not show the "feathering" of the schlieren image. The shock is quite clear in the PLIF image since the fluorescence levels map out the temperature levels in the flow. The temperature jump across the shock is quite apparent. Unfortunately, the signal levels for this experiment were not sufficient to show the expansion fan from the rearward-facing step, and the high signal region in the center of the flow is due to scattering from particulate (subsequent tests have removed the particulate from the flow).

A more exciting comparison is given by Figs. 10 and 11 which compare schlieren and NO PLIF results for helium injection. Once again the schlieren field of view is for a full tunnel height, the lower left edge of the image is 30 mm from the rearward-facing step, and the window nonidealities are as

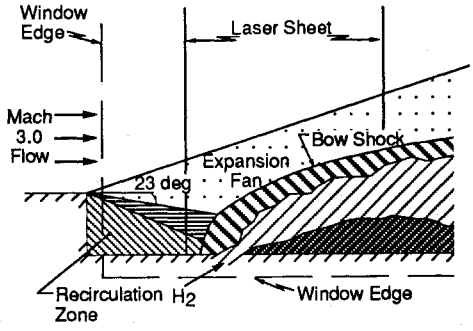

Fig. 7 Shock-tunnel flowfield with injection along the centerline of the tunnel.

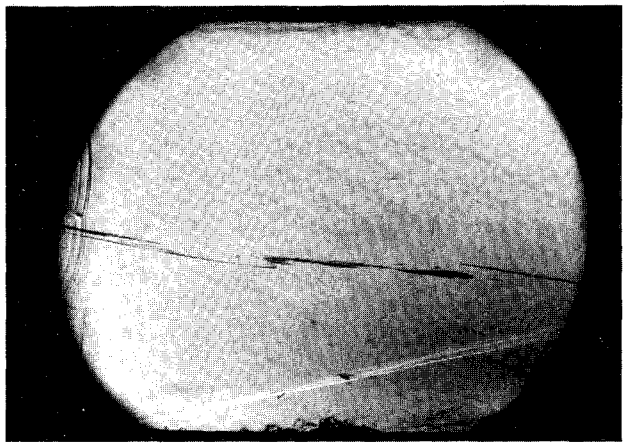

Fig. 8 Schlieren image of the recompression shock; T = 1360 K and P = 29 kPa.

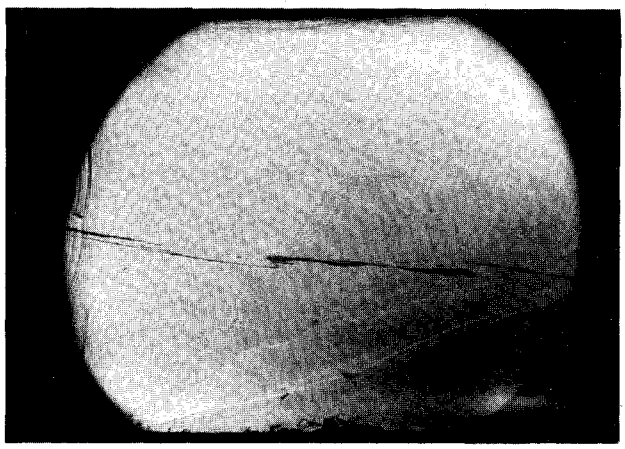

Fig. 10 Schlieren image with helium injection; T = 1370 K and P = 30 kPa.

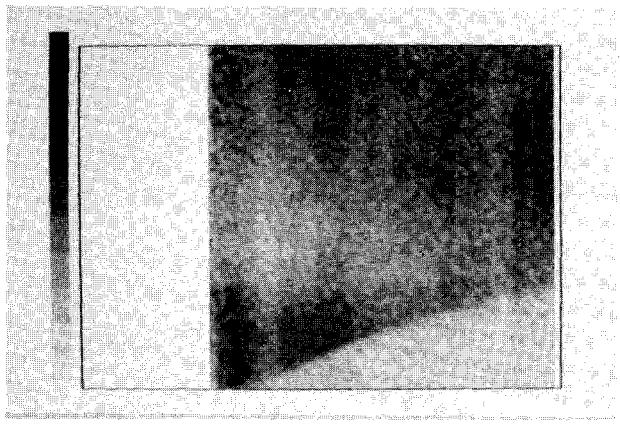

Fig. 9 PLIF image of the recompression shock; T = 1430 K and P = 34 kPa.

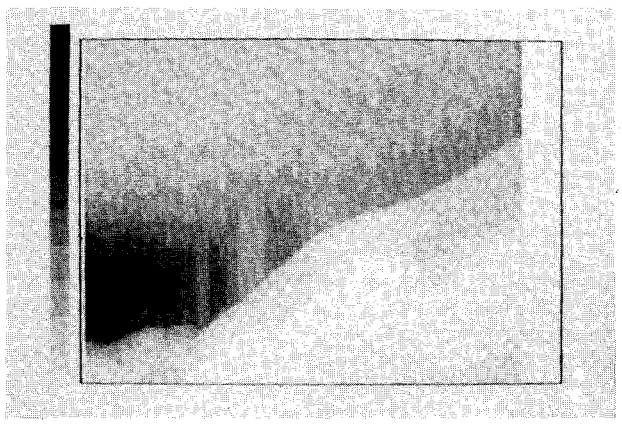

Fig. 11 NO PLIF image with helium injection; T = 1370 K and P = 30 kPa.

previously described. The schlieren result clearly shows the bow shock which is on the centerline of the tunnel and is due to the helium injectant plume. In addition, the Schlieren image shows the recompression shock that is unaffected by the injector away from the tunnel centerline. It is interesting to note the longitudinal waviness of the bow shock in the schlieren image which is an indicator that the position of the shock front varies slightly over time. Figure 11 shows an NO PLIF image of the flowfield with helium injection (pump transition $R_{11} + Q_{21}(13)$. This image represents 38 mm of flow length, extends upward 29 mm, and the rearward-facing step is 20-mm upstream of the left side of the image. The signal levels are an inverse temperature map spanning a range from ~550 to ~2000 K in the region immediately across the bow shock. The freestream temperature for this image was 1320 K. Wide vertical bars in the center of the image signify saturation of the pixels by the fluorescence signal due to a bright region in the intensity distribution of the laser sheet. The expansion fan can clearly be seen in this image and is represented by the shift from white to black starting at the upper left corner of the image, and appearing as radial contours, centered at the rearward-facing step to the left of the image. The bow shock appears as a distinct interface after the expansion fan. The NO fluorescence signal decreases sharply across the bow shock because of the increasing temperature (from ~550 to ~2000 K), and disappears near the interface with the helium plume where the NO number density drops below our minimum detectable limit.

A comparison of the bow shock and mixing region as determined by the schlieren and NO PLIF images illustrates that the two diagnostics are in very good agreement in terms of the spatial location of the bow shock. In addition, since the PLIF image is from the tunnel centerline, it definitively shows the bow shock to be centered in the tunnel; this was postulated but not proven by the schlieren image. Finally, both images show that the bow shock does not meet the tunnel wall, which implies that the recirculation zone may extend to the base of the injector. The PLIF image also defines the edge of the unmixed jet in the flow and shows that it too is a wavy interface.

Figure 12 is an OH PLIF image [pump transition $Q_1(7)$] for a flow with hydrogen injection. Flow conditions were identical to those for the NO PLIF image, and the field of view is as previously described. The OH bearing regions are clearly shown by the gray and black regions in this image. Comparison with Fig. 11 shows that the OH bearing zones are on the periphery of the jet or in the mixing regions between the jet and the bow shock. This illustrates that the combusting and noncombusting flows are qualitatively similar. The peak fluorescence intensities in this image correspond to a peak OH number density of $\approx 10^{15}$ molecules/cm^3 and $\approx 10^{14}$ of OH is also observable in the recirculation zone. The OH appears very near to the injector outlet on the leading edge of the jet. An ignition time for the jet can be approximated by comparing the ignition length (1.1 cm) to the exit velocity of the jet (1200 m/s) to yield a time of ≈ 10 μs. Given the very high temperatures behind the bow shock ($\approx$2000 K), a very short ignition time can be expected. This indicates that combustion of hydrogen and air in these very high temperature flows is a mixing limited process. The OH filament on the periphery of the fuel jet in Fig. 12 supports this conclusion.

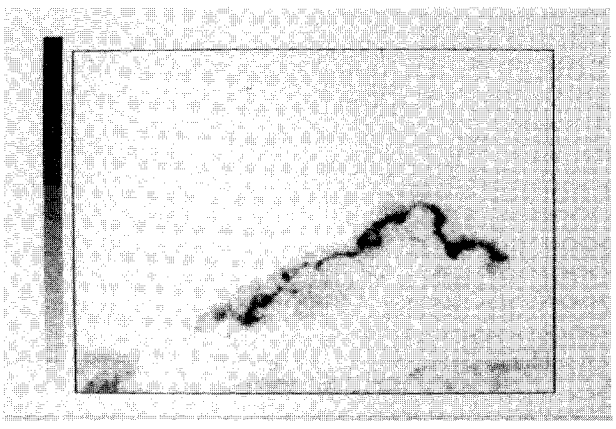

Fig. 12 OH PLIF image with H_2 injection; T = 1370 K and P = 30 kPa.

In addition to the previously described images, an emission image from the downstream window illustrated in Fig. 2 was used to define the spreading of the combustion zone after the injector station. This image was sensitive to emission from the OH A-X transition, and therefore, represents both chemically and thermally populated OH A-state radiation. The image illustrates that at 17.5 step-heights downstream of the center of the injection zone, combustion has spread across 55% of the tunnel height (3.85 step-heights). This implies a spreading rate of 0.22 for this position of the flow. The local spreading rate was found across this image to be 0.13. This value is much closer to that determined in other experiments[16] and implies that the overall spreading rate of 0.22 must be due to the initial penetration of injectant at the injector outlet. Using a spreading rate of 0.13, the number of duct heights required for the reaction zone to reach the top wall may be estimated to be 6. Therefore, an absolute minimum aspect ratio for a combustor with this style of injection is also 6.

Finally, pressure measurements on the top wall of the tunnel (up to 270 mm from the rearward-facing step) are identical for experiments with and without injection. Clearly, optical measurement methods provide a new insight into this region of the flow.

An exceptionally interesting comparison is afforded by contrasting this work with that of Abbitt et al.[17] which employs a similar rearward-facing step/injector configuration. The primary difference in the two experimental investigations are the stagnation temperatures; greater than 3000 K for this work and approximately 650 K for the work of Abbit et al.[17] Reacting flow results at a stagnation temperature of 650 K are dramatically different from those at 3500 K. The reaction zone for the low-temperature case is sufficiently intense to cause the expansion fan over the rearward-facing step to be replaced with an oblique shock. In addition, the recirculation zone and regions surrounding the injectors are shown to contain large quantities of OH which indicates combustion along the tunnel floor surrounding the injectors. This result is in marked contrast to our observations of thin flame sheets at the injector edge. One can speculate that the primary reason for the differences in the two studies is the stagnation temperatures which were employed. The high stagnation temperature device appears to operate in a mixing limited fashion. No ignition source is required and combustion proceeds along the interface which is swept down the duct. These results underscore the importance of testing at stagnation temperatures similar to those that will be experienced in the hypersonic flight envelope.

Conclusions and Recommendations

This article has described an experimental effort which developed both a high-enthalpy flow facility and successfully applied optical diagnostic measurement techniques to the nonreacting and reacting flowfield. A shock tunnel was designed, assembled, and verified to produce Mach 3.0 flows with stagnation pressures and temperatures of 1.0–5.0 MPa and 3000–4000 K. Schlieren, NO infrared emission, and NO and OH PLIF were developed and demonstrated on the high-enthalpy reacting flow facility. The NO and OH PLIF images were shown to be useful in describing both temperature and mixing properties of the flowfield (using NO), and as direct means of identifying reaction zones (using OH). The OH PLIF images were particularly useful in identifying combustion zones which were not measurable using conventional wall

pressure measurements. Thermal and chemiluminescent emission from OH were shown to be useful as a line-of-sight imaging measurement. Combustion results from this work indicate prompt ignition of the hydrogen jet (approximately 10 μs) and a local spreading rate of 0.13 was observed downstream of the injection zone. Therefore, the duct length required for the reaction to spread across the entire flow is approximately six duct heights given the injector configuration described in the report.

In addition to the direct conclusions just enumerated, this work has demonstrated the effectiveness of advanced diagnostic methods for monitoring scramjet processes. The benefits from these types of measurements to the development of high-speed flight vehicles can range from an evaluation of flow quality to direct assessments of the injection and mixing region that are critical to scramjet performance. Clearly, using the techniques and flow facility described in this article, a very complete study of supersonic reacting and nonreacting flows could be performed and would provide fundamental information regarding the flowfield and its mixing and reacting behavior, as well as producing direct measurements of the effectiveness of different injector configurations. Future work, using nonintrusive measurements, will undoubtedly contribute greatly to scramjet and/or high-speed flight combustor development.

Acknowledgments

This work was supported by the Air Force Wright Laboratory under a Phase II SBIR Contract F33615-88-C-2907, John Smith, Contract Monitor.

References

[1]McMillin, B. K., Palmer, J. L., and Hanson, R. K., "Planar Laser-Induced Fluorescence Imaging of Shock Tube Flows with Vibrational Nonequilibrium," AIAA Paper 91-1670, June 1991.

[2]Cassady, P. E., and Lieberg, S. F., "Planar Laser-Induced Fluorescence Measurements in Hypersonic Air Flowfield," AIAA Paper 91-1492, June 1991.

[3]Lee, M. P., and McMillin, B. K., Palmer, J. L., and Hanson, R. K., "Planar Fluorescence Imaging of a Transverse Jet in a Supersonic Cross Flow," AIAA Paper 91-0460, Jan. 1991.

[4]Hartfield, R. J., Hollo, S. D., and McDaniel, J. C., "Experimental Investigation of a Supersonic Swept Ramp Injector Using Laser-Indice Iodine Fluorescence," AIAA Paper 90-1518, June 1990.

[5]Smith, M. W., and Northam, G. B., "Instantaneous Planar Visualization of Reacting Supersonic Flows Using Silane Seeding," AIAA Paper 91-1690, June 1991.

[6]Cohen, L. S., Coulter, L. J., and Egan, W. J., "Penetration and Mixing of Multiple Gas Jets Subjected to a Cross Flow," *AIAA Journal*, Vol. 9, No. 4, 1971, pp. 718–724.

[7]Kee, R. J., Miller, J. A., and Jefferson, T. H., "CHEMKIN: A General Purpose, Problem Independent, Transportable, Fortran Chemical Kinetics Code Package," Sandia Lab., SAND 80-8003, Albuquerque, NM, 1980.

[8]Billig, F. S., "Current Problems in Non-Equilibrium Gas Dynamics SCRAMJET Engines," AIAA Professional Study Seminar on Gas Dynamics, Buffalo, NY, June 1989.

[9]Allen, M. G., Parker, T. E., Reinecke, W. G., Legner, H. H., Foutter, R. R., and Rawlins, W. T., "Instantaneous Temperature and Concentration Imaging in Supersonic Air Flow Behind a Rear Facing Step with Hydrogen Injection," AIAA Paper 92-0137, Jan. 1992.

[10]Rawlins, W. T., Parker, T. E., Foutter, R. R., and Allen, M. G., "Path Averaged Number Density and Temperature in High Enthalpy, Supersonic Air Flows by Time-Resolved Infrared Emission Spectroscopy," AIAA Paper 92-0140, Jan. 1992.

[11]Cavolowsky, J. A., private communication, NASA Ames Research Center, Moffett Field, CA, July 1991.

[12]Roshko, A., and Thonke, G. T., "Observations of Turbulent Reattachment Behind an Axisymmetric Downstream-Facing Step in Supersonic Flow," *AIAA Journal*, Vol. 4, No. 6, 1966, pp. 975–980.

[13]Stein, A., "Supersonic Flow Separation on a Backward Facing Step," Rept. No. AS66-18, Air Force Office of Scientific Research Grant 268-66, Bollin AFB, Washington, DC, 1966.

[14]Sirleix, M., Mirande, J., and Deleny, T., "Basic Experiments on the Reattachment of a Supersonic Stream," Royal Aircraft Establishment, Library Translation No. 1196, UK, Nov. 1965.

[15]Hortzaiker, J. R., "An Experimental Investigation of the Affect of the Approaching Boundary Layer on the Separated Flow Behind a Downstream Facing Step," National Aerospace Lab., NLR TR 700334, The Netherlands, June 1970.

[16]Hall, J. L., Dimotakis, P. E., and Rosemann, H., "Some Measurements of Molecular Mixing in Compressible Turbulent Shear Layers," AIAA Paper 91-1719, June 1991.

[17]Abbitt, J. D., McDaniel, J. C., Drauss, R. H., Whitehurst, R. B., and Segal, C., "Experimental Investigation of a Supersonic Combustion Flowfield Employing Staged Transverse Injection Behind a Rearward Facing Step," AIAA Paper 92-0090, Jan. 1992.